京 都 大 学 防 災 研 究 所 年 報　第48号 C　平成17年3月
Annuals of Disas. Prev. Res. Inst., Kyoto Univ., No. 48 C, 2005

Earthquake-Induced Catastrophic Landslide Risk Evaluation in Liquefiable Soils

Aurelian C. TRANDAFIR* and Kyoji SASSA

*COE Researcher, DPRI, Kyoto University

Synopsis

This paper outlines a methodology for evaluating the likelihood of catastrophic landslide occurrence on gentle slopes in liquefiable soils during earthquake. The approach is based on a modified Newmark sliding block model of assessing the earthquake-induced undrained landslide displacements for conditions of no shear stress reversals on the sliding surface. By employing the shear resistance-displacement relationship from undrained monotonic ring shear tests, the simulation model incorporates the sensitivity of computed displacements to variations in yield acceleration. The proposed approach involves an examination of undrained seismic slope performance under various horizontal seismic waveforms scaled to different specific values of the peak earthquake acceleration. An example problem illustrates how the proposed methodology may be used to demarcate, based on the magnitude of permanent seismic displacement, the levels of low, moderate and high risk of catastrophic landslide on a gentle slope in a saturated cohesionless soil susceptible to liquefaction during earthquake.

Keywords: earthquakes; slopes; liquefiable soil; catastrophic landslide hazard

1. Introduction

Catastrophic landslides occurred repeatedly on gentle slopes in urban areas during past earthquakes in Japan causing significant environmental damage and posing serious threat to inhabitants' lives. The January 1995 Nikawa landslide (Hyogo Prefecture), January 1995 Takarazuka landslide (Hyogo Prefecture) or May 2003 Tsukidate landslide (Miyagi Prefecture) are representative examples of such seismically-induced catastrophic slope failures. Typically, the sliding surface of these landslides was comprised of saturated cohesionless materials, and the slope gradient was greater than 10° but not exceeding 20°.

Laboratory studies consisting of undrained ring shear tests on soil samples from Nikawa (Sassa, 1996) and Tsukidate (Trandafir and Sassa, 2004) landslides revealed a gradual loss in undrained shear resistance after failure with progress of shear displacement. This so-called "sliding surface liquefaction" phenomenon (Sassa, 1996) culminated in undrained ultimate steady state strengths smaller than static (gravitational) driving shear stress on the sliding surface of the investigated landslides. Thus, the experimental results demonstrated the susceptibility of the sliding mass to an accelerated motion under static conditions (i.e., catastrophic failure) if the shear strength loss due to some transient disturbance (e.g., earthquake) was large enough to bring definitively the shear resistance on the sliding surface below the gravitational driving shear stress.

The sensitivity of undrained yield resistance to progressive shear displacement noted in the case of previously mentioned landslides, suggests that a performance-based methodology is necessary to assess the slope vulnerability against an earthquake-induced catastrophic failure, rather than a pseudo-static traditional limit equilibrium approach based on the concept of safety factor. Accordingly, a modified formulation of the Newmark (1965) sliding block model was developed by Trandafir and Sassa (2004, 2005) to assess the earthquake-induced undrained displacements on shear surfaces in a saturated cohesionless soil for conditions of no shear stress reversals on the sliding surface.

Basically, under conditions of no shear stress reversals, a catastrophic failure will take place when the earthquake-induced shear displacement exceeds a critical level associated with a definitive drop of undrained shear strength to a value equal to the gravitational (static) driving shear stress, and smaller yield resistances characterize the undrained shear behavior of the soil beyond this stage of deformation (Trandafir and Sassa, 2004, 2005). However, seismic stability analyses carried out for various hypothetical infinite slopes by using the modified Newmark

sliding block procedure (Trandafir and Sassa, 2005) revealed that estimated permanent displacements smaller than the critical value should also be regarded as dangerous for the post-earthquake slope serviceability. In this framework, the present paper describes, via an example problem, a performance-based approach that could be used to evaluate for conditions of no shear stress reversals the earthquake-induced catastrophic landslide hazard on shear surfaces in liquefiable soils.

2. Example Problem

The present numerical study is conducted for the case of Tsukidate landslide triggered by the 26-May-2003 Sanriku-Minami earthquake in Tsukidate town, Miyagi Prefecture, Japan. This translational slide with a volume of about 10,000 m^3 is characterized by a horizontal traveling distance of about 180 m, and a maximum velocity of about 6–7 m/sec (Konagai et al., 2003). The landslide occurred on a gentle slope of about 14°, and according to the post-earthquake reconnaissance survey, failure took place along a shear surface located in fully saturated silty sand.

2.1 Features of slide mass used in dynamic calculations

The configuration of Tsukidate slide mass before failure is shown in Fig. 1*a*. However, in order to be able to study the seismic slope performance in undrained conditions, the geometry from Fig. 1*a* is approximated by the equivalent infinite slope model depicted in Fig. 1*b*. The main reason for this approximation is that the material on the sliding surface is a liquefiable soil showing a significant amount of generated excess pore pressure even at the incipient stages of deformation, and a gradual loss in undrained strength after failure (Fig. 4) due to excess pore pressure built-up with progressive shear displacement. As noted later, for the infinite slope model shown in Fig. 1*b*, the shear resistance-displacement curve derived from the monotonic ring shear test TM2 in Fig. 4 was employed to perform the undrained dynamic calculations. This relationship incorporates the effects of excess pore pressure generation on the soil undrained shear strength. On the other hand, the influence of initial effective normal stress, σ'_0, and driving shear stress, τ_0, on the liquefaction resistance of saturated cohesionless soils, attested by several researchers (e.g., Castro, 1969; Kramer and Seed, 1988; Vaid et al., 1995; Ishihara et al., 1999; Matsuo et al., 2002; Sivathayalan and Vaid, 2002), is also representative for the material on the sliding surface of Tsukidate landslide (see Fig. 4). Obviously, for the real geometry of the investigated failure mass (Fig. 1*a*), the distribution of the initial (static) stresses (σ'_0, τ_0) generated by the gravitational forces is non-uniform along the actual sliding surface. Thus, after dividing the sliding mass in an appropriate number of slices and assuming, eventually, a uniform distribution of the initial stresses (σ'_0, τ_0) at the base of each slice, we would need to obtain the undrained yield resistance-displacement curves (such as the relationships in Fig. 4) for every combination of initial stresses (σ'_0, τ_0) encountered at the base of the slices within the slide mass.

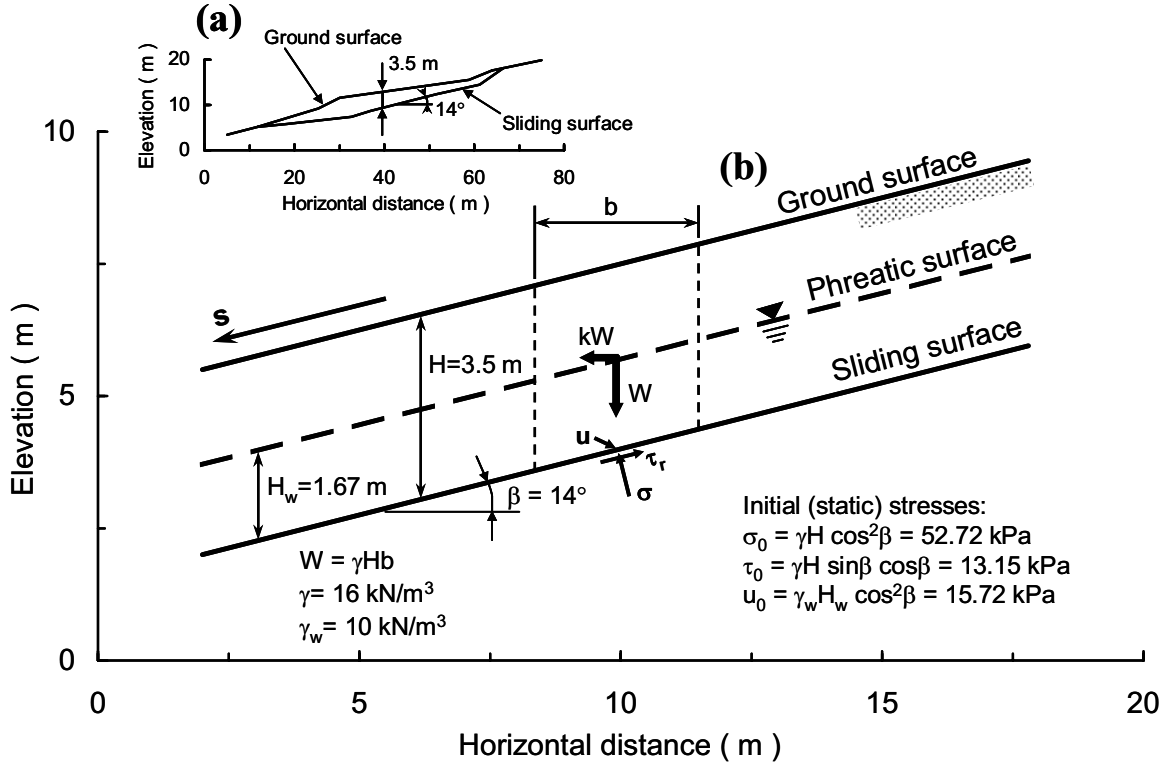

Fig. 1 Infinite slope characteristics (*b*) derived from the original configuration of the slide mass (*a*)

These curves would enable us to estimate and update the undrained yield acceleration of the slide mass based on the undrained yield resistances mobilized at the base of the slices along the sliding surface at a specific shear displacement during earthquake. However, such an approach requires a generalized soil model that could reproduce the undrained shear behavior (and provide the undrained yield resistance-displacement relationship) for any combination of initial stresses (σ'_0, τ_0). The development of a soil model for the undrained monotonic shear behavior, especially in the ring shear apparatus, represents a quite difficult task, and at present, such model is not available. As an alternative, the equivalent infinite slope model (Fig. 1*b*) was considered for the seismic stability analysis carried out in undrained conditions. For the particular geometry of the investigated translational landslide (Fig. 1*a*), this simplification seems quite reasonable, and offers the advantage of a uniform distribution of stresses along the sliding surface under static conditions, which may be described by a single pair of values (σ'_0, τ_0), as seen in Fig. 1*b*. Consequently, for a given location of the groundwater table, only one undrained monotonic ring shear test was necessary to obtain the undrained yield resistance-displacement relationship required for the seismic stability analysis. The groundwater level considered in Fig. 1*b* is relatively close to the location of the phreatic surface found in the field at sites adjacent to Tsukidate landslide.

2.2 Equation of motion for undrained conditions on the sliding surface

Assuming the slide mass in Fig. 1*b* as a rigid body in translation driven downslope by a horizontal seismic force, the equation of motion may be written as (Trandafir and Sassa, 2005)

$$\ddot{s} = (a - k_y\, g)\, \cos\beta \qquad (1)$$

where $\ddot{s}$ represents the relative acceleration on the direction parallel to the sliding surface, β is the infinite slope angle, while a, g and k_y stand for the horizontal earthquake acceleration, gravitational acceleration and yield coefficient, respectively. The horizontal earthquake acceleration coefficient, k, rendering the inertia force, kW, in a soil column of width b and weight W (Fig. 1*b*), represents the ratio between the horizontal earthquake acceleration and gravitational acceleration (i.e., $k=a/g$). It is worth mentioning that parameters a and consequently, $\ddot{s}$ in Eq. (1) are functions of time, t (i.e., $a=a(t)$, $\ddot{s}=\ddot{s}(t)$).

The horizontal yield coefficient for undrained conditions on the sliding surface is given by the following equation (Trandafir and Sassa, 2005):

$$k_y = \left(\frac{\tau_r}{\tau_0} - 1\right) \tan\beta \qquad (2)$$

Equation (2) makes use of the shear resistance-displacement relationship from undrained monotonic shearing (Fig. 2) in order to update the value of the undrained yield coefficient of the slide mass at a specific value of shear displacement during earthquake. The laboratory study introduced in the subsequent section, addressing the undrained monotonic and cyclic shear behavior of the soil on the sliding surface of Tsukidate landslide, comes to support the accuracy of using (in dynamic calculations) the shear resistance-displacement relationship from undrained monotonic shearing as an estimate of the undrained yield resistance during earthquake for conditions of no shear stress reversals on the sliding surface. The step-by-step numerical integration procedure to calculate the dynamic displacements given the expression of relative acceleration, $\ddot{s}$, is explained in detail elsewhere (Trandafir and Sassa, 2005).

Trandafir and Sassa (2004) investigated the influence of the vertical component of earthquake acceleration on the undrained seismic performance of the sample slope depicted in Fig. 1*b*. According to the computational results, the accuracy of estimated undrained seismic displacements was not significantly affected by neglecting in dynamic calculations the vertical component of earthquake acceleration. In these circumstances, the simplification made in the present study by considering only the horizontal component of earthquake acceleration seems reasonable.

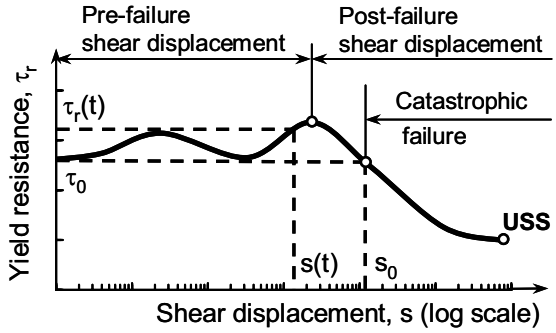

Legend: **USS** – Ultimate Steady State

Fig. 2 Example of undrained monotonic ring shear test result showing a progressive loss in undrained shear resistance after failure with increasing shear displacement

The example of undrained monotonic shear response shown in Fig. 2 corresponds to a saturated cohesionless soil possessing an ultimate steady state strength after failure smaller than static driving shear stress, τ_0. For materials on the sliding surface exhibiting this type of undrained shear behavior, a shear displacement at the end of seismic excitation exceeding the amount s_0 depicted in Fig. 2 is regarded in this paper as a "catastrophic failure" since the sliding mass is expected to develop an accelerated

motion even after the earthquake loading has ceased, due to the static driving shear stress exceeding the undrained yield resistance on the slip surface.

2.3 Undrained shear behavior of the soil on the sliding surface

An experimental study based on ring shear tests was undertaken to investigate the undrained shear behavior of the soil on the sliding surface under monotonic and cyclic loading conditions. Undrained ring shear tests with initial shear stress were carried out on soil specimens collected from the source area of Tsukidate landslide, by using the undrained torque–controlled ring shear apparatus DPRI-6 developed by Sassa and colleagues (Sassa et al., 2003). The samples tested in DPRI–6 may have a maximum height of 135 mm, and an outer and inner diameter of 350 mm and 250 mm, respectively. All the parameters of interest are monitored during the experiment by transducers, while two personal computers are used for test control and data recording. The ring shear tests by DPRI–6 can be carried out either in shear–torque control mode or shear speed control mode. Concerning the shear–torque control mode, three rotating gears are available capable to develop due to an accelerated motion a maximum shear speed on the median circumference of the specimen of 10 mm/sec, 32.3 cm/sec, and 2.24 m/sec, respectively. DPRI–6 is capable of reproducing undrained monotonic as well as undrained cyclic loading conditions, with cyclic total normal stresses and cyclic driving shear stresses within a range of frequencies up to 5 Hz.

The undrained ring shear tests for this study were conducted in shear–torque control mode using the medium rotating gear associated with a maximum shear speed on the median circumference of the specimen of 32.3 cm/sec. Due to the limited capacity of the shear box, the grains with a size greater than 4.75 mm were removed from the tested specimens since this fraction is negligible among the solid particles of the analyzed soil. Based on the grain size distribution curve shown in Fig. 3, the tested material from the sliding surface of Tsukidate landslide may be characterized as a silty sand with a fines content of about 26%. The soil samples for the undrained ring shear tests were prepared by dry deposition, saturation being accomplished by aid of carbon dioxide and de-aired water after setting-up the sample into the shear box.

Table 1 summarizes the experimental conditions for the undrained ring shear tests performed on the soil specimens from Tsukidate landslide. The experiments were conducted for the same initial shear stress, τ_0, and various initial effective normal stress levels on the sliding surface, as seen in Table 1.

Regarding the procedure for setting-up the initial stresses, the saturated soil specimen was consolidated first at an effective normal stress equal to the value of σ_0 in Table 1. Table 1 also gives the dry density, ρ_d,

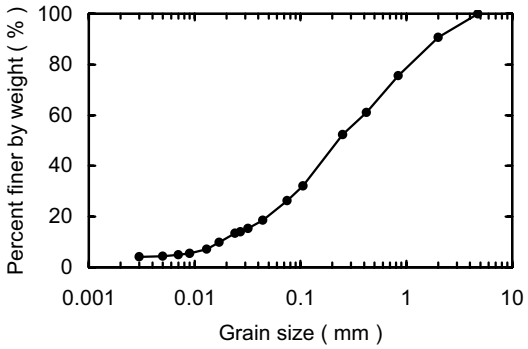

Fig. 3 Grain size distribution curve of the soil on the shear surface of Tsukidate landslide

calculated after consolidation, which is relatively close to the average value of dry density estimated for the soil on the sliding surface in the field, i.e., 1.1 g/cm^3. The specific gravity of the tested soil is about 2.27. After consolidation, the shear stress acting on the specimen was increased in drained conditions with a loading rate of about 0.2 kPa/sec to the initial value τ_0 given in Table 1. In the case of tests TM1, TM3 and TC1, after applying the initial shear stress, τ_0, the shear box was shifted to undrained conditions and the soil specimen was sheared either in a monotonic or cyclic manner, as noticed in Table 1. In the case of test TM2, after setting-up the initial shear stress, τ_0, a back pressure of 15.75 kPa has been applied before undrained monotonic shearing. This situation is equivalent with a rise in groundwater level until 1.67 m above the sliding surface in Fig. 1*b*. Consequently, the soil specimen in test TM2 became somewhat overconsolidated, with an over-consolidation ratio of about 1.43 before starting the undrained monotonic shearing.

Table 1 Summary of undrained ring shear tests on soil specimens from Tsukidate landslide

Testing condition	Test no.	ρ_d (g/cm^3)	σ_0 (kPa)	τ_0 (kPa)	u_0 (kPa)
Monotonic	TM1	1.141	52.39	13.15	0.00
Monotonic	TM2	1.132	52.29	13.15	15.75
Monotonic	TM3	1.121	70.34	13.15	0.00
Cyclic	TC1	1.136	52.48	13.15	0.00

The undrained monotonic ring shear tests were performed by gradually increasing the shear stress with a loading rate of about 0.2 kPa/sec in undrained conditions, while maintaining constant the total normal stress. Failure of the specimens during shearing resulted in an accelerated motion until the shear velocity reached the limit value of 32.3 cm/sec. Figure 4 shows the results from undrained monotonic shearing in terms of effective stress path and shear resistance-displacement relationship. Prior to failure, the tested soil demonstrated a quasi steady state type of shear response (Ishihara, 1993) during tests TM1 and TM2, while the behaviour during test TM3 may

be described as strain hardening (Fig. 4). After failure, the soil exhibited, in all tests, a gradual loss in strength with progress of shear displacement. This phenomenon is addressed as sliding surface liquefaction (Sassa, 1996), and is illustrated in Fig. 4 by an effective stress path moving down along the failure line towards the ultimate steady state (*USS*). As it may be noticed in Fig. 4, the effects associated with sample overconsolidation in test TM2 when compared to the data from test TM1, consist of an increase in peak friction angle in the stress space and a more sudden transition to quasi steady state after attaining the first peak in the shear resistance–displacement representation.

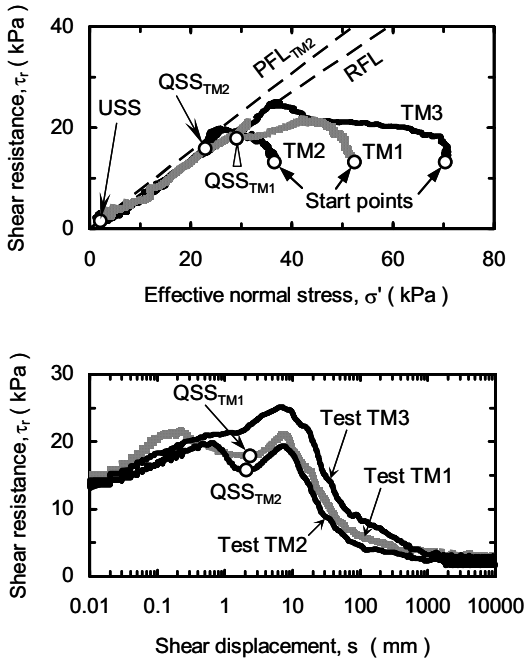

Fig. 4 Results of undrained monotonic ring shear tests on soil specimens from Tsukidate landslide

The time history of applied cyclic stresses for the undrained cyclic ring shear test TC1 were selected in order to simulate the dynamic conditions on the sliding surface of the infinite slope from Fig. 1*b* subjected to a horizontal seismic excitation of sinusoidal shape with the characteristics given in Fig. 5. To be able to compare the shear responses under monotonic and cyclic loading conditions, the same initial stresses were applied in tests TM1 and TC1, as noticed in Table 1. The total normal stress, σ, and driving shear stress, τ_d, during cyclic testing were obtained from the following equations, provided the value of the earthquake acceleration coefficient, k, at a certain instant:

$$\sigma = \sigma_0 - k\tau_0 \quad (3)$$

$$\tau_d = \tau_0 + k\sigma_0 \quad (4)$$

Figure 6 shows the total normal stress and cyclic shear resistance in relation to shear displacement for the undrained cyclic ring shear test TC1, as well as the corresponding shear resistance–displacement curve obtained from undrained monotonic shearing under the same initial stress conditions (i.e., test TM1). A quick examination of the experimental results from Fig. 6 reveals that the upper boundary of the unloading–reloading loops describing the cyclic shear resistance measured during test TC1 follows very closely the shear resistance-displacement relationship from undrained monotonic shearing.

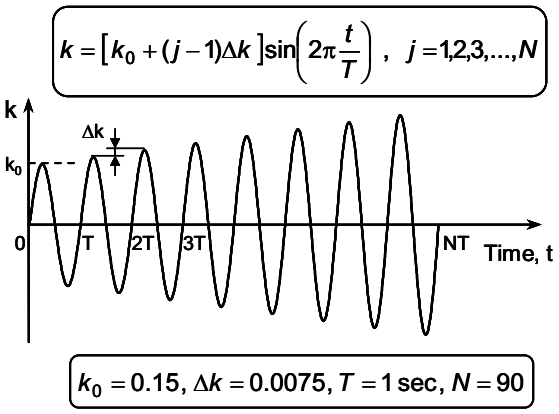

Fig. 5 Characteristics of horizontal seismic excitation used in the undrained cyclic ring shear test TC1 on the soil specimen from Tsukidate landslide

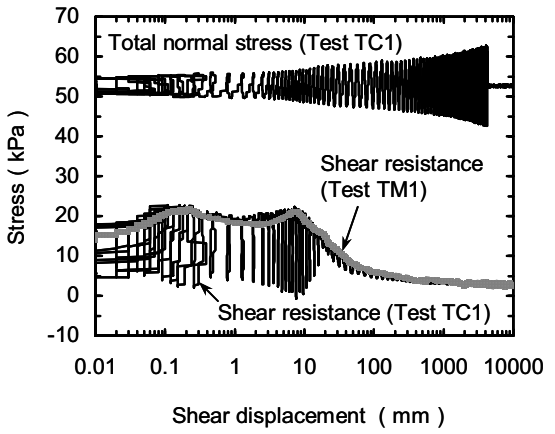

Fig. 6 Undrained cyclic shear behavior of the soil on the shear surface of Tsukidate landslide, and the corresponding undrained monotonic shear response

This experimental outcome clearly demonstrates that, for conditions of no shear stress reversals on the sliding surface, the yield resistance of tested soil is insensitive to variations in total normal stress during cyclic shearing. Furthermore, as seen from the unloading-reloading loops of measured cyclic shear resistance during test TC1 (Fig. 6), the soil behavior during yielding before failure is predominately plastic except the initial stages of deformation at very small shear displacements (e.g., < 0.1 mm) which are

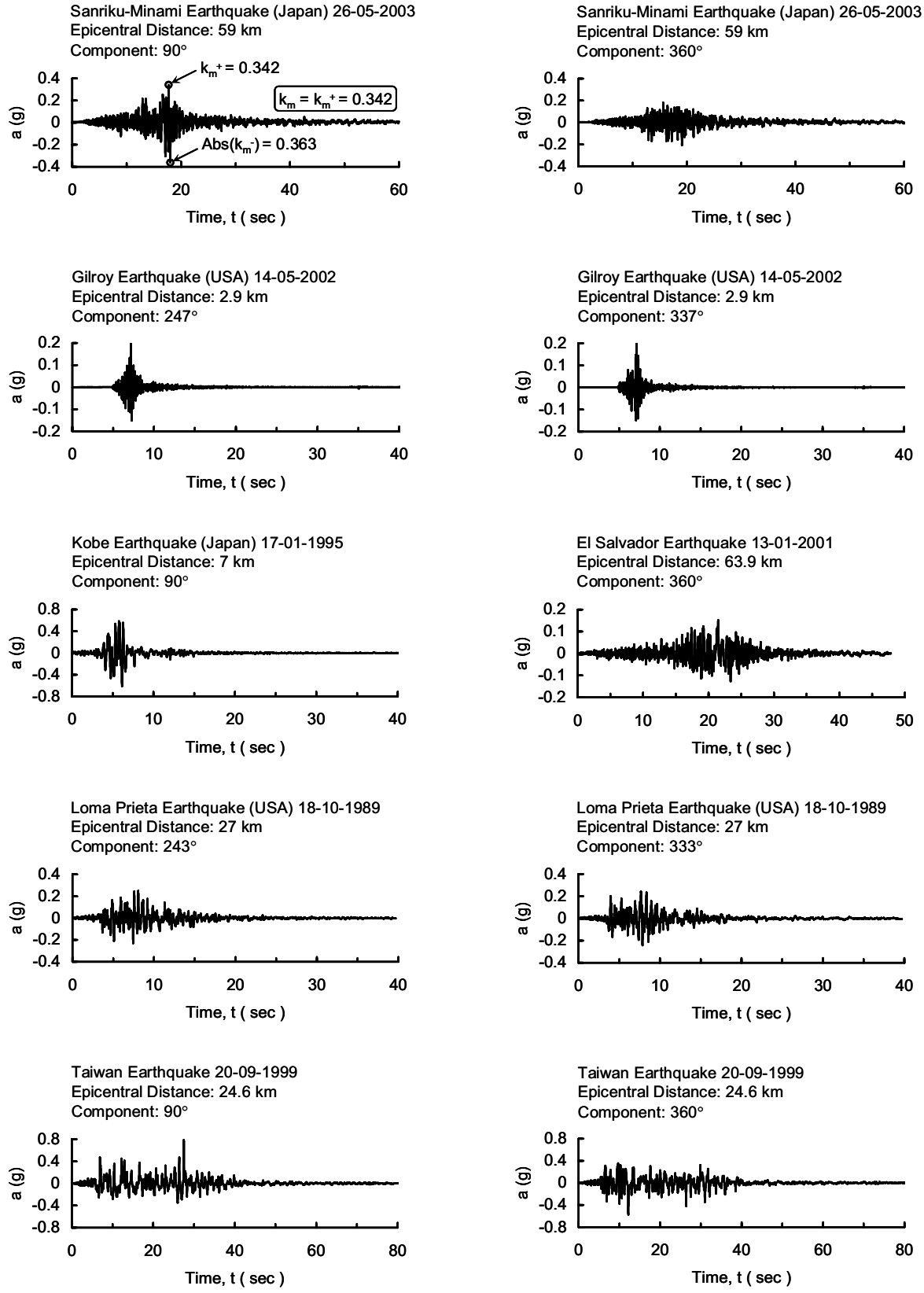

Fig. 7 Input earthquake records

beyond the scope of this study. Thus the rigid–plastic assumption adopted for the entire shear resistance–displacement curve from undrained monotonic shearing including, therefore, the interval of shear displacements before failure, seems reasonable in an undrained seismic analysis based on the modified Newmark formulation described in the previous section.

The initial stress conditions for the undrained monotonic ring shear test TM2 (Table 1) correspond to the infinite slope characteristics shown in Fig. 1*b*. Accordingly, the shear resistance-displacement curve from test TM2 in Fig. 4 was employed in the following numerical investigation. This relationship indicates a critical shear displacement, s_0, necessary to induce a catastrophic failure of about 18 mm.

2.4 Input seismic records

The undrained seismic performance of the sliding mass shown in Fig. 1*b* was investigated using ten input horizontal earthquake records depicted in Fig. 7. Each seismic record was scaled to different specific values of the peak earthquake acceleration, $k_m g$, and the corresponding earthquake-induced undrained permanent displacements were estimated. As illustrated in Fig. 7, the peak earthquake acceleration ($k_m g$) is defined in this study as the maximum value of earthquake acceleration on the positive side of an input accelerogram, irrespective of whether this value is smaller or greater than the maximum absolute value of earthquake acceleration on the negative side of the accelerogram. Positive values of the accelerograms shown in Fig. 7 are associated in this analysis with horizontal inertia forces due to earthquake driving the sliding mass downslope; thus corresponding to the direction of *kW* shown in Fig. 1*b*. For all of the numerical results presented herein, the condition of no shear stress reversals on the sliding surface (which is essential in the applicability of the previously introduced sliding block formulation) was satisfied during the calculated dynamic response.

3. Operation Charts

Figure 8 provides the relationship between the earthquake-induced undrained permanent displacement, s_p, (relative to the critical displacement, s_0=18mm) and the acceleration ratio, k_{yp}/k_m, for three input seismic records (i.e., Gilroy (337°), Gilroy (247°) and Sanriku-Minami (90°)). k_{yp} (= constant = 0.127) stands for the peak yield coefficient in undrained conditions obtained by substituting in Eq. 2 the corresponding values of the peak undrained strength, τ_r^p (=19.82 kPa derived from the shear resistance-displacement data corresponding to test TM2 in Fig. 4), τ_0 and β (Fig. 1b), whereas k_m represents the peak earthquake acceleration coefficient of the scaled input seismic record. Due to the non-linear nature of the diagrams depicted in Fig. 8, this type of chart may be utilized to differentiate for a particular slope, the levels of risk associated with the onset of a catastrophic landslide during earthquake. Apparently, for permanent displacements in excess of $0.53s_0$ (i.e., zone III in Fig. 8), the relationships start to increase asymptotically towards the critical level s_0 with subsequent decrease in the acceleration ratio, indicating that from this stage of deformation, insignificantly larger peak accelerations ($k_m g$) could trigger a catastrophic landslide. Therefore, estimated permanent displacements exceeding $0.53s_0$ should be regarded as unsafe, and associated with a high risk of catastrophic failure. The slide mass could be considered safe against a catastrophic shear failure if the calculated earthquake-induced permanent displacement is smaller than $0.3s_0$ (i.e., zone I in Fig. 8), whereas estimated permanent displacements located within the transition interval ranging from $0.3s_0$ to $0.53s_0$ (i.e., zone II in Fig. 8) should represent a warning signal indicating the necessity for a careful evaluation of the dynamic stability of the analyzed slope.

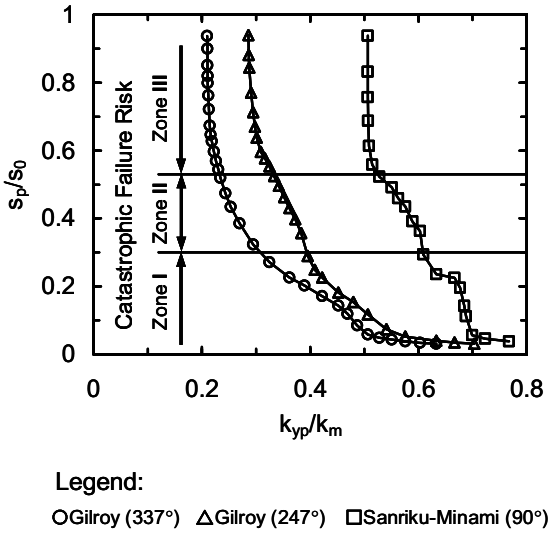

Fig. 8 Earthquake-induced permanent displacement, s_p, (relative to the critical displacement, s_0) versus acceleration ratio, k_{yp}/k_m

We define the critical peak earthquake acceleration, $k_{mc}g$, as the peak earthquake acceleration required to induce an undrained permanent displacement equal to the critical displacement, i.e., $s_p=s_0$. Hence, $k_{mc}g$ stands for the minimum peak earthquake acceleration necessary to trigger a catastrophic failure. We also define the $k_{ms}g$ parameter as the value of the peak acceleration required to trigger a permanent displacement of $0.3s_0$ which represents the upper limit of zone I (i.e., safe zone) in Fig. 8.

As the displacement curves from Fig. 8, determined for different earthquake records, approach

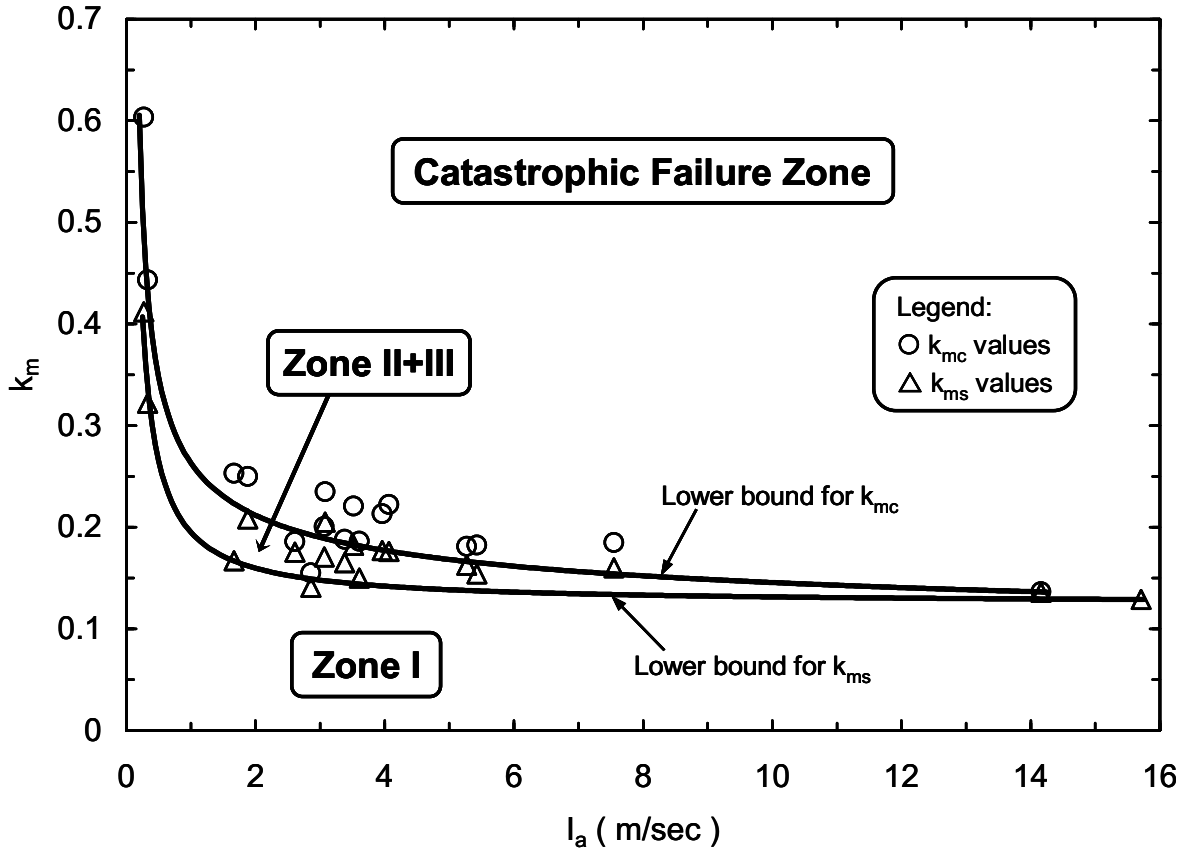

Fig. 9 Coefficients of peak earthquake acceleration k_{mc} and k_{ms} (required to trigger levels of permanent displacement equal to s_0 and $0.3s_0$, respectively) in relation to Arias intensity, I_a, estimated for the corresponding seismic records scaled to $k_m g = 0.5g$

the s_0 and $0.3s_0$ levels at different acceleration ratios, it appears that, for the analyzed slope, k_{mc} and k_{ms} depend strongly on the characteristics of the input accelerogram. In the present investigation, the k_{mc} and k_{ms} parameters were estimated for all of the seismic records shown in Fig. 7, considering both the positive and negative orientations of each accelerogram. For the considered earthquakes, these data were compiled in relation to the Arias intensity parameter, I_a, as seen in Fig. 9. Arias intensity represents a commonly used energy-based measure of earthquake shaking severity, and offers the advantage of incorporating both the amplitude and duration elements of ground motion, as well as all frequencies of recorded motion. For a single component of motion in a given direction, Arias intensity (I_a) is defined as (Arias, 1970)

$$I_a = \frac{\pi}{2g} \int_0^{t_s} a^2(t)\, dt \qquad (5)$$

where t_s represents the duration of earthquake-shaking. The Arias intensity values used in the diagram given in Fig. 9, were estimated by Eq. (5) from the input accelerogram scaled to a peak acceleration ($k_m g$) of $0.5g$. In this representation, the lower bounds of k_{mc} and k_{ms} values are used to separate the regions of peak earthquake accelerations that may cause a catastrophic failure, bring the slope near the brink of a catastrophic failure (i.e., zone II+III in Fig. 9) or on the contrary, showing no danger for the post-earthquake slope serviceability (i.e., zone I in Fig. 9). The diagram illustrated in Fig. 9, offers the advantage of a quick assessment of the earthquake-induced catastrophic landslide hazard by knowing only the characteristics of the design earthquake (i.e., k_m and I_a).

4. Conclusions

The performance-based approach described in this paper may be used to identify unacceptable permanent deformations, and estimate the minimum peak earthquake acceleration that could endanger the stability of gentle slopes in liquefiable soils susceptible to catastrophic failure under seismic conditions. By employing an easy-to-use sliding block model of evaluating the undrained seismic displacements, the proposed methodology represents for the practitioners a useful tool in performing quick and yet quantitative preliminary assessments of the earthquake-induced catastrophic landslide hazard. This information may be useful in deciding whether a more refined stability analysis based on

comprehensive field and laboratory investigations, as well as numerical studies using more complex computational techniques (e.g., finite element method) should be undertaken in a subsequent stage to evaluate, in a more accurate manner, the slope vulnerability and eventually plan the mitigation measures against an earthquake-induced catastrophic failure.

References

Arias, A. (1970): A measure of earthquake intensity, Seismic design for nuclear power plants, Edited by R.J. Hansen, MIT Press, Cambridge, Mass.

Castro, G. (1969): Liquefaction of sands, Ph.D. thesis, Harvard University, Cambridge, Mass.

Ishihara, K. (1993): Liquefaction and flow failure during earthquakes, Géotechnique, Vol. 43, No. 3, pp. 351-415.

Ishihara, K., Tsukamoto, Y., and Nakayama, S. (1999): Flow-type failure of slopes based on behavior of anisotropically consolidated sand, Proc. Int. Symp. Slope Stability Engng–IS-SHIKOKU'99, Matsuyama, Shikoku, Japan, Vol. 1, pp. 3-12.

Konagai, K., Ito, H., and Johansson, J. (2003): Features of Tsukidate landslide mass in the May 26, 2003, South-Sanriku earthquake, Proc. 42nd Annual Conf. Japan Landslide Society, Toyama, Japan, 20-21 August, Vol. 1, pp. 233-236.

Kramer, S.L., and Seed, H.B. (1988): Initiation of soil liquefaction under static loading conditions, Journal of Geotechnical Engineering, ASCE, Vol. 114, No. 4, pp. 412-430.

Matsuo, O., Saito, Y., Sasaki, T., Kondoh, K., and Sato, T. (2002): Earthquake-induced flow slides of fills and infinite slopes, Soils and Foundations, Vol. 42, No. 1, pp. 89-104.

Newmark, N.M. (1965): Effects of earthquakes on dams and embankments, Géotechnique, Vol. 15, No. 2, pp. 139-159.

Sassa, K. (1996): Prediction of earthquake induced landslides, Proc. 7th Int. Symp. Landslides, Trondheim, Norway, 16-21 June, Vol. 1, pp. 115-132, Rotterdam, Balkema.

Sassa, K., Wang, G., and Fukuoka, H. (2003): Performing undrained shear tests on saturated sands in a new intelligent type of ring shear apparatus, Geotechnical Testing Journal, ASTM, Vol. 26, No. 3, pp. 257–265.

Sivathayalan, S., and Vaid, Y.P. (2002): Influence of generalized initial state and principal stress rotation on the undrained response of sands. Canadian Geotechnical Journal, Vol. 39, No. 1, pp. 63-76.

Trandafir, A.C., and Sassa, K. (2004): Newmark deformation analysis of earthquake-induced catastrophic landslides in liquefiable soils, Proc. 9th Int. Symp. Landslides, Rio de Janeiro, June 28-July 2, Vol. 1, pp. 723-728, Rotterdam, Balkema.

Trandafir, A.C., and Sassa, K. (2005): Seismic triggering of catastrophic failures on shear surfaces in saturated cohesionless soils, Canadian Geotechnical Journal, Vol. 42, No. 1, pp. 229-251.

Vaid, Y.P., Sivathayalan, S., Uthayakumar, M., and Eliadorani, A. (1995): Liquefaction potential of reconstituted Syncrude sand, Proc. 48th Canadian Geotech. Conf., Vancouver, B.C., Vol. 1, pp. 319-330.

地震時において液状化地盤で発生する地すべりの危険度評価

オーレリアン　カタリン　トランダフィル*、佐々恭二

*京都大学防災研究所　COE 研究員

要旨

この研究では，ゆるい砂質土等で構成される緩斜面で地震時における大規模地すべりの発生を評価する方法を提案する。この手法は，すべり面においてせん断力の反転が起きない条件での地震による非排水性の地すべり変位を評価した「修正 Newmark 法」に基づいている。この方法は，非排水単調載荷リングせん断試験によって得られるせん断抵抗―変位関係を用いて，降伏加速度を変化させた場合に計算される変位の感度をシミュレーションモデルに組み込んだものである。この研究では，修正 Newmark 法をベースに最大加速度が異なる様々な横揺れ地震波の下での非排水条件の斜面の挙動を考慮する。そして適用例として，恒久的な地震変位のもとでどのような基準により緩斜面での地震による大規模地すべりの危険度（大・中・小）が設定できるかを示す。

キーワード：地震、 斜面、 液状化地盤、 大規模地震災害

C13

Earthquake-induced catastrophic landslide risk evaluation in liquefiable soils

○Aurelian C. Trandafir・Kyoji Sassa

１．はじめに

日本では過去，地震時において緩斜面で大規模地すべりが繰り返し発生しており，地域社会に大きなダメージを与えるとともに住民の生命を脅かしている。1995 年 1 月に発生した仁川地すべり（兵庫県）および 2003 年 5 月に発生した築館地すべり（宮城県）は地震によって引き起こされた地すべりの代表的な例である。これらの地すべりのすべり面は飽和非粘着性土によって構成され，斜面勾配は 10°～20°の間である。地震によって引き起こされた大規模地すべりの源頭部で採取されたサンプルを用いた非排水条件下でのリングせん断試験の結果，せん断変位が進行するとともに非排水せん断強度がゆるやかな減少することが明らかになった。この液状化現象では最終的に静的せん断力（駆動力）よりも小さい定常状態強度に収束した。このことは，地震などによるせん断強度の低下ですべり面のせん断抵抗が重力によるせん断力以下となった場合，潜在地すべり土塊が静的条件のもとで加速する可能性を示している。そこでこの研究では，ゆるい砂質土等で構成される緩斜面で地震時における大規模地すべりの発生を評価する方法を提案する。この手法は，すべり面においてせん断力の反転が起きない条件での地震による非排水性の地すべり変位を評価した「修正 Newmark 法」に基づいている。この方法は，非排水単調載荷リングせん断試験によって得られるせん断抵抗―変位関係を用いて，降伏加速度を変化させた場合に計算される変位の感度をシミュレーションモデルに組み込んだものである。この研究では，修正 Newmark 法をベースに最大加速度が異なる様々な横揺れ地震波の下での非排水条件の斜面の挙動を考慮する。そして適用例として，恒久的な地震変位のもとでどのような基準により緩斜面での地震による大規模地すべりの危険度（大・中・小）が設定できるかを示す。

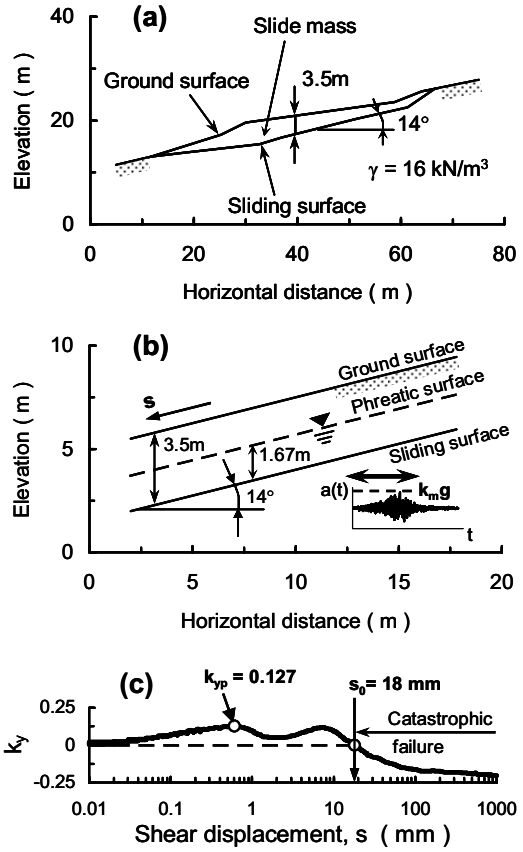

Fig. 1. (*a*) Configuration of Tsukidate slide mass before failure; (*b*) features of the equivalent infinite slope model; and (*c*) undrained yield coefficient of the slide mass used in the seismic analysis.

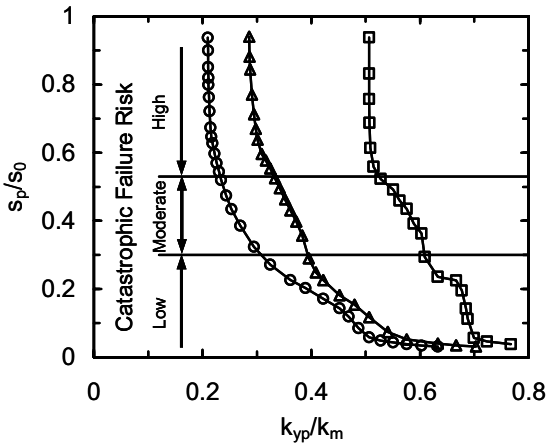

Fig. 2. Earthquake-induced permanent displacement, s_p, (relative to s_0) versus acceleration ratio, k_{yp}/k_m, for various seismic records.